

Personalized Subgraph Federated Learning with Sheaf Collaboration

Wenfei Liang^{a,*}, Yanan Zhao^a, Rui She^a, Yiming Li^a and Wee Peng Tay^a

^aSchool of Electrical and Electronic Engineering, Nanyang Technological University, Singapore

Abstract. Graph-structured data is prevalent in many applications. In subgraph federated learning (FL), this data is distributed across clients, each with a local subgraph. Personalized subgraph FL aims to develop a customized model for each client to handle diverse data distributions. However, performance variation across clients remains a key issue due to the heterogeneity of local subgraphs. To overcome the challenge, we propose *FedSheafHN*, a novel framework built on a sheaf collaboration mechanism to unify enhanced client descriptors with efficient personalized model generation. Specifically, FedSheafHN embeds each client’s local subgraph into a server-constructed collaboration graph by leveraging graph-level embeddings and employing sheaf diffusion within the collaboration graph to enrich client representations. Subsequently, FedSheafHN generates customized client models via a server-optimized hypernetwork. Empirical evaluations demonstrate that FedSheafHN outperforms existing personalized subgraph FL methods on various graph datasets. Additionally, it exhibits fast model convergence and effectively generalizes to new clients.

1 Introduction

Many graph neural networks (GNNs) focus on a single graph [36, 50], storing nodes and edges from various sources in a central server. Collaborative training of GNNs across distributed graphs can be achieved through federated learning (FL) [49, 30], where each participant trains a local GNN, and a central server aggregates their updated weights. In practice, clients may have unique subgraphs, and local data distributions can vary significantly. Some clients may even tackle distinct tasks. Personalized federated learning (PFL) [37] addresses this by allowing each client to use a personalized rather than a shared model.

This paper focuses on subgraph FL, a particularly challenging setting where **clients hold largely disjoint subsets of a global graph**. A key challenge is balancing the benefits of joint training with maintaining unique models tailored to the local data and task of each client. Recent subgraph FL methods [49, 3] attempt to address this by either addressing missing edges across subgraphs, e.g., by expanding subgraphs using information from others, or by identifying community structures to guide model aggregation. However, as shown in Fig. 1(a), **existing PFL methods suffer from significant performance variation across clients**, largely due to the heterogeneity of subgraphs from different parts of a global graph. We ask the following two questions:

Q1 How can we learn and exploit the underlying relationships among clients to support effective joint training?

Q2 How can we maintain personalized models when clients have distinct subgraphs and data distributions?

* Corresponding Author. Email: wenfei001@e.ntu.edu.sg.

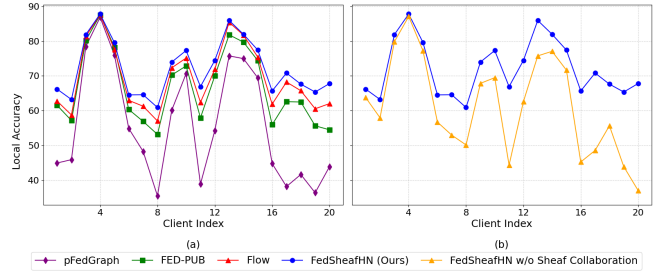


Figure 1. Local accuracy comparison across 20 clients in non-overlapping scenario on the ogbn-arxiv dataset. (a) Comparison with PFL baselines: Flow, FED-PUB, and pFedGraph, demonstrating more stable and balanced performance among all clients for FedSheafHN. (b) Comparison shows FedSheafHN with sheaf collaboration (71.88 ± 7.92) outperforms the variant without it (61.26 ± 13.77), highlighting the effectiveness of sheaf collaboration.

To address **Q1**, we propose sheaf collaboration, which enables effective cross-client collaboration by leveraging a server-side collaboration graph as a manifold to model underlying client relationships. This facilitates both information exchange and progressive refinement of client descriptors. To address **Q2**, we employ Hypernetworks (HNs) to generate client-specific model parameters from descriptive vectors, enabling flexibility and diversity in personalized client models. The HNs map input embedding to model parameters, effectively constraining all personalized models to lie on a shared manifold in the parameter space [34]. This ensures each client’s model is adapted to its data while still maintaining a structured space for generalization.

We call our model *Federated learning with Sheaf collaboration and HyperNetworks* (FedSheafHN). FedSheafHN facilitates in-depth cross-client information exchange and generates highly personalized models from enriched client representations. Rather than relying on single-scalar similarity or partial parameter sharing, sheaf collaboration leverages the underlying structure of the client relationship and captures rich, client-specific mappings that align local distributions without sacrificing individuality, as demonstrated in Fig. 1(b). By equipping these enriched representations with HNs, FedSheafHN provides a promising approach to the core personalization challenges while producing models better aligned to heterogeneous demands, ultimately offering more stable and balanced performance for all clients. Our main contributions are summarized as follows:

- We propose sheaf collaboration framework that leverages sheaf diffusion with server-constructed collaboration graph to capture the intricate inter-client relationships, thereby enabling more effective information aggregation across heterogeneous clients.
- We develop an attention-based HNs and optimize it batch-wise on

the server, efficiently generating personalized model parameters using enriched client descriptions produced by sheaf collaboration.

- We provide a theoretical analysis of FedSheafHN, establishing both convergence and generalization guarantees.
- We conduct extensive experiments on multiple graph-structured datasets under heterogeneous subgraph FL scenarios. FedSheafHN consistently outperforms state-of-the-art baselines in most cases, while converging quickly and generalizing effectively to newly joined clients.

Notations: For a positive integer N , we let $[N] = \{1, 2, \dots, N\}$. A matrix \mathbf{A} is written as $\mathbf{A} = (\mathbf{a}_i)_{i \in [N]}$ if its i -th row is the row vector \mathbf{a}_i , for $i = 1, 2, \dots, N$. A vectorized version of \mathbf{A} is denoted as $\tilde{\mathbf{A}}$, which is formed by stacking the transposes of the row vectors \mathbf{a}_i for $i = 1, 2, \dots, N$ into a single vector. $(\cdot)^\top$ denotes the transpose operator. A graph G is denoted as $G = (\mathcal{N}, \mathcal{E})$ where \mathcal{N} is the vertex set and \mathcal{E} is the edge set, or $G = (\mathcal{N}, \mathcal{E}, \mathcal{F})$ if it is associated with a feature matrix \mathcal{F} . \oplus denotes the direct sum of vector spaces.

2 Related work

2.1 Federated Learning

PFL To address challenges related to data and device heterogeneity in FL, various PFL methods have been introduced, encompassing various approaches such as local fine-tuning [2, 31], regularization for objective functions [11, 45], model mixing [24], meta-learning [15, 20], personalized parameter decomposition [2, 28], and differentially privacy [1, 22]. Additionally, the concept of training multiple global models at the server has been explored for efficient PFL [9, 14]. This method involves training different models for distinct client groups, and clustering clients based on similarity. Another strategy is to train individual client models collaboratively [14, 48, 46, 40, 32].

Graph FL Recent research highlights the potential of integrating the FL framework into collaborative GNNs training, focusing on subgraph- and graph-level methods. Graph-level FL assumes that clients have disjoint graphs, such as molecular graphs. Studies [43, 12, 38] delved into addressing heterogeneity in non-IID graphs with varying labels. In contrast to graph-level FL, subgraph-level FL introduces unique challenges related to graph structures, such as missing links between subgraphs of a global graph. Methods like [42, 49] addressed this by augmenting nodes and connecting them, while [3] explored subgraph communities as densely connected clusters of subgraphs to address the problem. Unlike the aforementioned subgraph FL methods, our approach facilitates sheaf collaboration at the server to capture the underlying geometry and client interconnections, enabling effective representation for heterogeneous clients. This process can be considered as node-client two-level graph learning, improving the model’s capacity to capture and utilize diverse information.

2.2 Hypernetworks

HNs [18] are deep neural networks that generate weights for a target network. The output weights are dynamically adjusted based on the input to the HNs [19, 27]. SMASH [6] extended HNs to Neural Architecture Search (NAS) by encoding architectures as 3D tensors using a memory channel scheme. In contrast, our approach encodes networks as computation graphs and employs GNNs. GHN [47] was introduced for anytime prediction tasks, optimizing both speed and the speed-accuracy trade-off curve. pFedHN [34] leveraged HNs in FL with input task embeddings, while hFedGHN [44] extended GHN to train heterogeneous local models based on graph learning.

HNs inherently lend themselves to learn a diverse set of personalized models, and our approach equips them with an attention layer to further aggregate cross-client information, optimizing the HNs batch-wise to efficiently generate highly personalized model parameters from enriched client descriptions.

3 Methodology

3.1 The FedSheafHN Framework

We consider a FL scenario with N clients and a central server. Every client $i \in [N]$ possesses a local graph $G_i = (\mathcal{M}_i, \mathcal{E}_i, \mathbf{V}_i)$, where \mathcal{M}_i is the node set, \mathcal{E}_i is the edge set, and \mathbf{V}_i is a feature matrix. Denote $\mathbf{V}_i = (\mathbf{v}_{i,m})_{m \in \mathcal{M}_i}$, whose rows are the node feature vectors $\mathbf{v}_{i,m}$ for each node $m \in \mathcal{M}_i$. Each client aims to learn a local model, denoted as $f_i(G_i; \omega_i)$, tailored to its specific task. Here, ω_i represents the model parameters for the client i . It is important to note that each local graph G_i can potentially be a subgraph of a larger, undisclosed global graph.

FedSheafHN aims to enhance the performance of the personalized model $f_i(G_i; \omega_i)$ on each client through subgraph FL. We refer the reader to Fig. 2 for an overview of the FedSheafHN pipeline. FedSheafHN constructs a collaboration graph G_s on the server using the client graph-level embeddings transmitted from clients. The server generates personalized model parameters $\omega_{b,i}^{(s)}$ for each client i using the sheaf diffusion model $S(\cdot; \theta)$ and hypernetwork $H(\cdot; \varphi)$. For ease of reference, we call $\omega_{b,i}^{(s)}$ the *backbone* parameter for client i . The server then distributes backbone parameters $(\omega_{b,i}^{(s)})_{i \in [N]}$ to clients.

The model parameters $\omega_i = (\omega_{b,i}, \omega_{h,i})$ of each client i are composed of two parts: the backbone parameter $\omega_{b,i}$ (initially trained locally and then updated by the server) and the head parameters $\omega_{h,i}$ (trained locally). Each client i initializes $\omega_{b,i} = \omega_{b,i}^{(s)}$ and $\omega_{h,i}$ as the previously trained head parameters (with random initialization before the first FL round). It then performs T_c epochs of local training on local graph G_i to update the model parameters ω_i . Let the model parameters after T_c epochs of local training be $\omega_i^{(c)} = (\omega_{b,i}^{(c)}, \omega_{h,i}^{(c)})$. Each client i transmits its incremental difference in its backbone parameter $\Delta \omega_{b,i} := \omega_{b,i}^{(c)} - \omega_{b,i}^{(s)}$ to the server. The server updates the sheaf diffusion model S and hypernetwork H . This process is repeated for multiple communication rounds.

The objective of each client i is to find

$$\arg \min_{\omega_i} \mathcal{L}_i(\omega_i), \quad (1)$$

where $\mathcal{L}_i(\cdot)$ denotes the task-specific loss of client i . The global training objective at the server is defined as

$$\begin{aligned} \arg \min_{(\omega_{b,i})_{i \in [N]}} \mathcal{L}((\omega_{b,i})_{i \in [N]}) &= \arg \min_{(\omega_{b,i})_{i \in [N]}} \sum_{i=1}^N \mathcal{L}_i(\omega_{b,i}, \omega_{h,i}^{(c)}) \\ &= \arg \min_{\theta, \varphi} \sum_{i=1}^N \mathcal{L}_i(\theta, \varphi, \omega_{h,i}^{(c)}), \end{aligned} \quad (2)$$

where the last equality holds because $\omega_{b,i}$ is function of sheaf diffusion parameters θ and hypernetwork parameters φ .¹

In the following subsections, we provide detailed descriptions of each component of the FedSheafHN framework.

¹ We abuse notations in Eq. (2) by writing the same symbol \mathcal{L}_i .

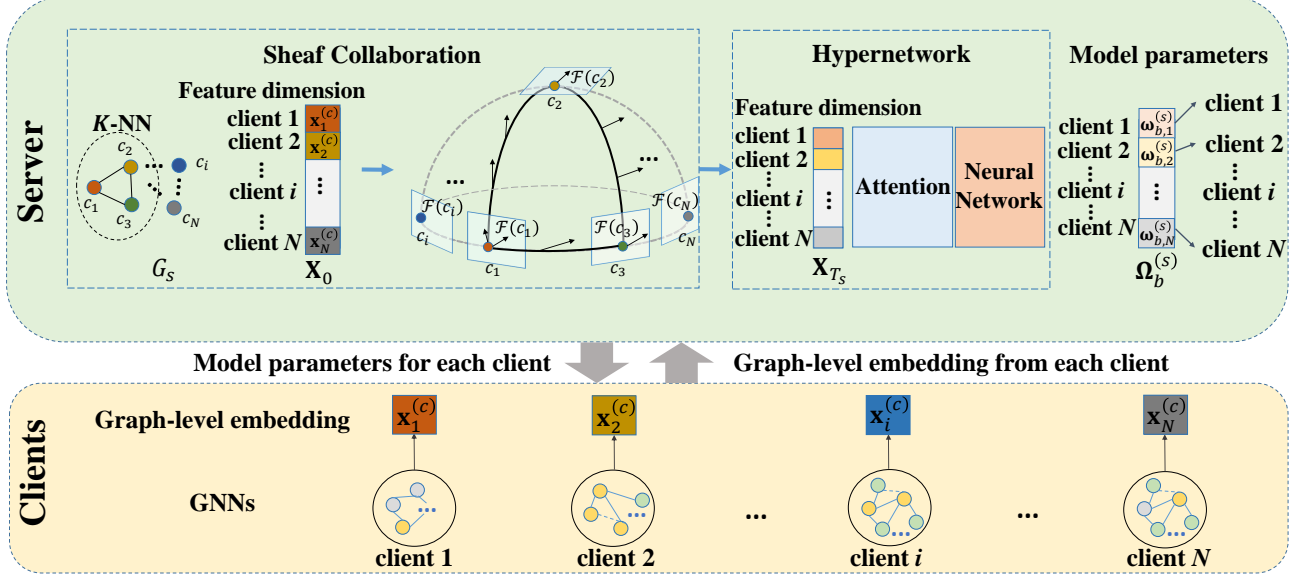


Figure 2. Overview of the FedSheafHN framework. Clients train GNNs to process local graph-structured data and generate graph-level embeddings. The server constructs a client collaboration graph from these embeddings to capture inter-client relationships. It updates the embeddings using sheaf diffusion, and then employs an attention-based hypernetwork to generate personalized model parameters based on the enriched client descriptions.

3.2 Sheaf Collaboration

Collaboration Graph Construction In subgraph FL, the server faces challenges in perceiving the overarching graph structure, complicating effective client collaboration. To address this, we formulate a novel collaboration graph leveraging client data-driven features to capture intrinsic geometric relationships. This graph facilitates client collaboration and enhances client-specific data representation.

Let $\mathbf{v}_{i,m}^{(c)}$ be the updated embedding vector of node $m \in \mathcal{M}_i$ of client i after T_c epochs local training of the client model $f_i(G_i; \omega_i)$. The graph-level embedding of client i is computed locally as

$$\mathbf{x}_i^{(c)} = \frac{1}{|\mathcal{M}_i|} \sum_{m \in \mathcal{M}_i} \mathbf{v}_{i,m}^{(c)}, \quad (3)$$

and transmitted to the server. It serves as the feature representation of client i . After receiving the graph-level embeddings from all clients, the server constructs a collaboration graph

$$G_s = ([N], \mathcal{E}_s, \mathbf{X}_0), \quad (4)$$

where \mathcal{E}_s is the edge set, and $\mathbf{X}_0 = (\mathbf{x}_i^{(c)})_{i \in [N]}$ is the feature matrix consisting of graph-level embeddings of all clients stacked in row form. The edge set is formed using a K -nearest neighbors (KNN) approach based on a predefined distance (e.g., cosine similarity) between the graph-level embeddings. To conserve communication resources, the client collaboration graph G_s on the server is updated every r_{in} communication rounds. Specifically, after r_{in} communication rounds, we reset \mathbf{X}_0 using the graph-level embeddings transmitted by the clients, i.e., $(\mathbf{x}_i^{(c)})_{i \in [N]}$.

Graph Representation Learning To uncover latent inter-client relationships and enrich client descriptions through information aggregation, our method incorporates elements of (cellular) sheaf theory. A cellular sheaf assigns a vector space to each node and edge in a graph, with linear maps for incident node-edge pairs [7, 10, 5]. These vector spaces represent points on a manifold, with the sheaf Laplacian modeling discrete transport of elements via rotations in neighboring vector spaces, where the graph acts as the manifold. Inspired by

this, our framework employs the server-side collaboration graph as a manifold to model client relationships.

Mathematically, a cellular sheaf (G_s, \mathcal{F}) on the collaboration graph G_s includes three components: (a) a vector space $\mathcal{F}(n)$ for each $n \in [N]$ containing the graph-level embedding vector of client n , (b) a vector space $\mathcal{F}(e)$ for each $e \in \mathcal{E}_s$, and (c) a linear map $\mathcal{F}_{n \leq e} : \mathcal{F}(n) \rightarrow \mathcal{F}(e)$ for each incident node-edge pair $n \leq e$. The map $\mathcal{F}_{n \leq e}$ is also known as a restriction map, which transports an element from the node space to the edge space. Therefore, for $(n, m) \in \mathcal{E}_s$, we can compute the difference between $\mathbf{x}_n \in \mathcal{F}(n)$ and $\mathbf{x}_m \in \mathcal{F}(m)$ via the restrictions $\mathcal{F}_{n \leq e} \mathbf{x}_n$ and $\mathcal{F}_{m \leq e} \mathbf{x}_m$ (both in $\mathcal{F}((n, m))$), capturing the relationship between two nodes.

For $\mathbf{X} = (\mathbf{x}_n)_{n \in [N]} \in \bigoplus_{n \in [N]} \mathcal{F}(n)$, the sheaf Laplacian of (G_s, \mathcal{F}) is a linear map that maps \mathbf{X} to $L_{\mathcal{F}}(\mathbf{X}) \in \bigoplus_{n \in [N]} \mathcal{F}(n)$, whose node or client n component is defined as

$$L_{\mathcal{F}}(\mathbf{X})_n := \sum_{n, m \leq e} \mathcal{F}_{n \leq e}^{\top} (\mathcal{F}_{n \leq e} \mathbf{x}_n - \mathcal{F}_{m \leq e} \mathbf{x}_m). \quad (5)$$

Let \mathbf{D} be the block-diagonal of $L_{\mathcal{F}}$. The normalized sheaf Laplacian is given by

$$\Delta_{\mathcal{F}} := \mathbf{D}^{-1/2} L_{\mathcal{F}} \mathbf{D}^{-1/2}. \quad (6)$$

This operator can be used to describe the process of vector space elements being transported and rotated into neighboring vector spaces, capturing the essence of element transitions within the sheaf.

We model the restriction map $\mathcal{F}_{n \leq e}$ using a multi-layer perceptron (MLP), which is updated with each server gradient update instance. We stack T_s layers of the sheaf diffusion model to evolve the client embeddings as shown in Fig. 3. Denote the sheaf diffusion model at layer $t \in [T_s]$ as

$$g(\cdot, \theta_t) = -\sigma(\Delta_{\mathcal{F}(t)}(\mathbf{I} \otimes \mathbf{W}_1^{(t)})(\cdot) \mathbf{W}_2^{(t)}), \quad (7)$$

where θ_t is the set of learnable parameters at layer t , including the learnable weight matrices $\mathbf{W}_1^{(t)}$ and $\mathbf{W}_2^{(t)}$ and the MLP weights for the restriction maps.

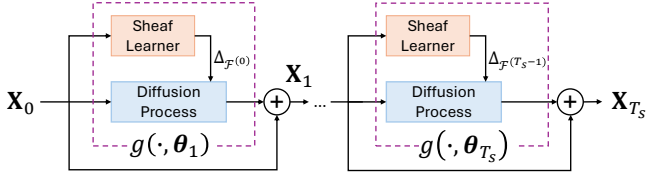


Figure 3. Sheaf diffusion model pipeline $S(\cdot; \theta)$. The evolution of the sheaf is described by a learnable function, enabling the model to utilize the latest available features to manipulate the underlying geometry of the graph.

The corresponding sheaf Laplacian is denoted as $\Delta_{\mathcal{F}(t)}$. The server adopts a diffusion-type model [5] to update the client graph-level embeddings as follows: for $t = 1, \dots, T_s$,

$$\mathbf{X}_t = \mathbf{X}_{t-1} + g(\mathbf{X}_{t-1}; \theta_{t-1}), \quad (8)$$

where $\sigma(\cdot)$ denotes a non-linear function, \mathbf{I} is the identity matrix, and \otimes is the Kronecker product.

The iteration Eq. (8) is performed for T_s times and its output is denoted as $S(\mathbf{X}_0; \theta)$, given by

$$\mathbf{X}_{T_s} := S(\mathbf{X}_0; \theta) = (\mathbf{x}_i^{(T_s)})_{i \in [N]}, \quad (9)$$

where $\theta = (\theta_t)_{t \in [T_s]}$.

The collaboration graph G_s evolves in tandem with client model training, with graph-level embeddings progressively refined to better represent client graph features. This process seamlessly integrates into client model training, requiring no additional models, and aligns the evolution of G_s with the adaptation of client models.

3.3 Optimization of the Hypernetwork

To generate personalized model parameters for each client, we utilize HNs taking the updated client graph-level embeddings \mathbf{X}_{T_s} from Eq. (9) as input. The HNs is optimized to generate personalized backbone parameters for all clients using the collaboration graph feature matrix.

Unlike conventional HNs that use a basic MLP [47, 34, 44] without explicit client relationships, using the embeddings from the neural sheaf diffusion model allows FedSheafHN to integrate potential latent relationships between the clients. To achieve this, the HNs denoted by $H(\cdot; \varphi)$ for our FedSheafHN incorporates an attention layer on top of a MLP, where the attention-based embedding is given by

$$\mathbf{X}_{T_s}^{\text{att}} = f_{\text{softmax}} \left((\mathbf{X}_{T_s} \mathbf{A}_{\text{att}}^Q) (\mathbf{X}_{T_s} \mathbf{A}_{\text{att}}^K)^\top \right) \mathbf{X}_{T_s} \mathbf{A}_{\text{att}}^V, \quad (10)$$

f_{softmax} denotes the row-wise softmax function, and $\mathbf{A}_{\text{att}}^Q$, $\mathbf{A}_{\text{att}}^K$, and $\mathbf{A}_{\text{att}}^V$ are all learnable matrices. Then, $\mathbf{X}_{T_s}^{\text{att}}$ is fed into the MLP to generate the backbone parameters.

In summary, the output of the HNs is given by

$$\Omega_b^{(s)} := H(\mathbf{X}_{T_s}; \varphi) = (\omega_{b,i}^{(s)})_{i \in [N]}, \quad (11)$$

where $\omega_{b,i}^{(s)}$ denotes the backbone parameters of client i , and φ are the HNs parameters, including attention layer and MLP.

3.4 Learning Procedure

After receiving $\omega_{b,i}^{(s)}$ from the server in the current communication round, each client i performs T_c rounds of local training to obtain the updated parameters $\omega_i^{(c)} = (\omega_{b,i}^{(c)}, \omega_{h,i}^{(c)})$. In each local training epoch,

the model parameters ω_i are updated using $\omega_i := \omega_i - \gamma \nabla_{\omega_i} \mathcal{L}_i(\omega_i)$, where γ is a hyperparameter. Each client i transmits $\Delta \omega_{b,i} := \omega_{b,i}^{(c)} - \omega_{b,i}^{(s)}$ to the server, forming $\Delta \Omega_b = (\Delta \omega_{b,i})_{i \in [N]}$.

To simplify notations, we represent our quantities of interest in vector form. We use $\tilde{\theta}$ and $\tilde{\varphi}$ to represent the vectorized versions of θ and φ , respectively. The vectorized version of \mathbf{X}_{T_s} in Eq. (9) is written as $\tilde{\mathbf{X}}_{T_s} := S(\tilde{\mathbf{X}}_0; \tilde{\theta})$. Similarly, the vectorized version of $\Omega_b^{(s)}$ in Eq. (11) is given by $\tilde{\Omega}_b^{(s)} := H(\tilde{\mathbf{X}}_{T_s}; \tilde{\varphi})$.

Using Eq. (2), we derive the gradients of FedSheafHN for the parameters $\tilde{\theta}$, $\tilde{\varphi}$ on the server via $\Delta \tilde{\Omega}_b$ and the chain rule. From [34], we have the update rule for the server's parameters:

$$\Delta \tilde{\theta} = \mathbf{J}_{\tilde{\theta}}(\tilde{\Omega}_b^{(s)}) \Delta \tilde{\Omega}_b, \quad (12)$$

$$\Delta \tilde{\varphi} = \mathbf{J}_{\tilde{\varphi}}(\tilde{\Omega}_b^{(s)}) \Delta \tilde{\Omega}_b. \quad (13)$$

We also have

$$\mathbf{J}_{\tilde{\theta}}(\tilde{\Omega}_b^{(s)}) = \mathbf{J}_{\tilde{\theta}}(S(\tilde{\mathbf{X}}_0; \tilde{\theta})) \mathbf{J}_{\tilde{\mathbf{X}}_{T_s}}(H(\tilde{\mathbf{X}}_{T_s}; \tilde{\varphi})), \quad (14)$$

as well as

$$\mathbf{J}_{\tilde{\varphi}}(\tilde{\Omega}_b^{(s)}) = \mathbf{J}_{\tilde{\varphi}}(H(\tilde{\mathbf{X}}_{T_s}; \tilde{\varphi})), \quad (15)$$

where $\mathbf{J}_{\tilde{\theta}}(\cdot)$ and $\mathbf{J}_{\tilde{\varphi}}(\cdot)$ are the Jacobians with respect to (w.r.t.) $\tilde{\theta}$ and $\tilde{\varphi}$, respectively. Throughout the training process, the parameters $\tilde{\theta}$ of the model S are updated according to Eq. (12) and Eq. (14) using the gradient descent step $\tilde{\theta} := \tilde{\theta} - \alpha \Delta \tilde{\theta}$, where α is a gradient control hyperparameter. The parameters $\tilde{\varphi}$ of the model H are updated according to Eq. (13) and Eq. (15) using $\tilde{\varphi} := \tilde{\varphi} - \beta \Delta \tilde{\varphi}$, where β is a hyperparameter. The full procedure of FedSheafHN is outlined in Algorithm 1 in Appendix A.2.

3.5 Theoretical Basis

Convergence Guarantees We provide guarantees by bounding the expected average gradient norm, with the detailed proof and complete formulation presented in Appendix B.

Theorem 1. *Under standard assumptions of smoothness and boundedness (cf. the Appendix), the optimization of FedSheafHN after T communication round satisfies*

$$\frac{1}{T} \sum_{t=1}^T \mathbb{E} \|\nabla \mathcal{L}(\omega_t)\|^2 \leq \frac{(\mathcal{L}(\omega_0) - \mathcal{L}^*)}{\sqrt{NT}} + \frac{LL_1(16\sigma_1^2 + 8T_c L_G^2)}{T_c \sqrt{NT}} + \frac{16NL_7^2 b_3^2 b_2^2}{T} + \frac{(L+2)}{T_c} b_1^2, \quad (16)$$

where \mathcal{L} denotes the global objective Eq. (2) with lower bound \mathcal{L}^* . ω_0 and ω_t are the initial and t -th communication round parameters. L, L_1, L_7 are smoothness constants. b_1, b_2, b_3 bound gradient norms. σ_1 bounds gradient variance, and L_G measures client dissimilarity.

Generalization Guarantees From Eq. (2), the expected loss is \mathcal{L} , and the empirical loss is denoted as $\hat{\mathcal{L}}$. All learnable parameters are assumed to be bound within a ball of radius R and satisfy global Lipschitz conditions for all potential functions in \mathcal{L} . The parameter space dimensions for $\mathbf{x}_i^{(c)}$, θ , φ , and $\omega_{h,i}$ are d_i, d_θ, d_φ , and $d_{\omega_{h,i}}$, respectively. L, L_s , and L_H are constants related to Lipschitz conditions. The proof is provided in Appendix C.

Theorem 2. *Suppose there are N clients, and each client i has a sample size larger than M , with $M = \mathcal{O}\left(d_i + \frac{d_\theta + d_\varphi + d_{\omega_{h,i}}}{N} \frac{1}{\xi^2} \log\left(\frac{RL(L_s + L_H + 1)}{\xi}\right) + \frac{1}{N\xi^2} \log \frac{1}{\delta}\right)$, it holds with probability at least $1 - \delta$ that $|\mathcal{L}(\omega_i) - \hat{\mathcal{L}}(\omega_i)| \leq \xi$.*

Table 1. Results on the non-overlapping node scenario. The reported results are mean and standard deviation over five different runs. The best and the second-best results are highlighted in bold and underlined, respectively. OOM refers to out-of-memory.

Methods	Cora		Citeseer		Pubmed	
	10 Clients	20 Clients	10 Clients	20 Clients	10 Clients	20 Clients
Local	71.26±0.29	74.65±0.42	67.82±0.13	65.98±0.17	82.81±0.39	82.65±0.03
FedAvg	72.38±2.45	69.81±13.28	65.71±0.37	63.08±7.38	79.88±0.07	78.48±7.65
FedProx	60.18±7.04	48.22±6.81	63.33±3.25	64.85±1.35	82.55±0.24	80.50±0.25
FedSage+	69.05±1.59	57.97±12.6	65.63±3.10	65.46±0.74	82.62±0.31	80.82±0.25
FGGP	66.57±0.56	54.58±0.83	60.99±0.68	57.13±0.33	76.84±0.59	73.08±0.81
FedPer	65.24±1.19	70.80±0.72	62.75±5.65	60.06±2.24	71.42±2.17	73.05±0.36
pFedHN	65.24±0.21	70.65±2.21	63.45±0.44	58.98±1.60	77.22±1.74	73.20±2.47
pFedGraph	76.57±1.37	76.61±0.63	71.61±0.64	67.43±0.49	80.38±0.30	80.48±0.58
FED-PUB	80.25±0.54	81.04±0.31	<u>73.42±0.75</u>	66.87±0.21	<u>85.95±0.77</u>	<u>85.38±0.82</u>
Flow	<u>81.81±0.14</u>	<u>81.42±0.18</u>	73.05±0.24	<u>70.01±0.24</u>	85.53±0.05	84.48±0.09
FedSheafHN (ours)	83.49±0.22	82.35±0.18	75.27±0.39	72.20±0.24	86.50±0.09	85.57±0.05

Methods	Amazon-Computer		Amazon-Photo		ogbn-arxiv	
	10 Clients	20 Clients	10 Clients	20 Clients	10 Clients	20 Clients
Local	85.90±0.35	87.79±0.49	76.21±1.34	81.93±0.59	64.92±0.09	65.06±0.05
FedAvg	66.78±0.00	71.44±0.08	79.61±3.12	82.12±0.02	48.77±2.88	42.02±17.09
FedProx	83.81±1.09	73.05±1.30	80.92±4.64	82.32±0.29	64.37±0.18	63.03±0.04
FedSage+	80.50±1.30	70.42±0.85	76.81±8.24	80.58±1.15	64.52±0.14	63.31±0.20
FGGP	66.91±1.24	48.25±0.85	68.52±0.53	54.85±0.57	OOM	OOM
FedPer	67.41±0.67	72.91±0.50	76.10±2.18	82.80±0.07	45.31±0.33	47.55±0.01
pFedHN	66.85±0.09	69.94±1.27	74.12±0.90	82.03±0.10	57.70±0.30	50.61±0.85
pFedGraph	66.45±0.83	71.57±0.36	74.57±1.05	84.04±0.50	56.37±0.31	56.19±0.83
FED-PUB	88.00±0.24	89.99±0.05	93.73±0.22	91.04±0.32	66.48±0.09	66.99±0.18
Flow	<u>88.67±0.12</u>	<u>90.31±0.11</u>	<u>93.94±0.07</u>	<u>92.24±0.10</u>	<u>68.91±0.04</u>	<u>69.89±0.11</u>
FedSheafHN (ours)	90.56±0.03	91.00±0.09	94.22±0.10	92.99±0.05	71.28±0.03	71.75±0.09

4 Experiments

We evaluate the performance of FedSheafHN on six datasets, focusing on node classification tasks within two distinct subgraph FL scenarios. We compare its performance with several state-of-the-art baselines using Federated Accuracy [34] as the metric, defined as $\frac{1}{N} \sum_{i \in N} \text{Acc}(f(G_i; \omega_i))$, where $\text{Acc}(\cdot)$ denotes the accuracy of the given model. The code is available at <https://github.com/CarrieWFF/FedSheafHN>.

4.1 Experimental Settings

Real-World Datasets Following experimental in [49, 3], we partition datasets into segments, assigning each client a dedicated subgraph. This allocation ensures that each participant manages a segment of a larger, original graph. Experiments are conducted on six datasets: Cora, CiteSeer [33], Pubmed, and ogbn-arxiv [13] for citation graphs, as well as Computer and Photo [25, 35] for Amazon product graphs. The partitioning of these datasets is executed through the METIS graph partitioning algorithm [16], with the number of subsets predetermined. Our experiments include both the non-overlapping and overlapping node scenarios. In the non-overlapping node scenario, the METIS output is directly utilized, creating distinct subgraphs without shared nodes, thus yielding a more heterogeneous setting. In the overlapping node scenario, the subgraphs are achieved by sampling smaller subgraphs from the initial METIS partitioned results. Dataset statistics are provided in Appendix A.1.

Baselines We compare our results with following baselines. The FL methods focus on training a global model, include FedAvg [26], FedProx [21], FedSage+ [49], and FGGP [39]. The PFL methods aim to provide personalized models for individual clients, include FedPer [2], pFedHN [34], pFedGraph [46], FED-PUB [3], and Flow [28].

Implementation Details The client models are two-layer GCNs for all baselines. The HN used in FedSheafHN consists of an attention layer and a two-layer MLP. The hidden dimension of GCNs and HNs is set to 128. The Adam optimizer [17] is applied for optimization. Data splits are 40% for training, 30% for validation, and 30% for testing. FL runs for 100 communication rounds on Cora, CiteSeer, Pubmed, and Computer, and 150 rounds on Photo and ogbn-arxiv, with 3 local epochs for Cora/CiteSeer, 15 for Pubmed, and 10 for the rest. In our framework, server updates G_s every $r_{in} = 5$ communication rounds. Hyperparameters used are given in Appendix A.3.

All experiments are conducted using PyTorch [29] and PyTorch Geometric [8] on NVIDIA GeForce RTX 3090. The runtime of FedSheafHN depends mainly on the number of clients, as client training is performed sequentially for simulation. Generally, training 50 clients with 3 local epochs over 100 total rounds takes around 3 hours, with memory usage varying from 300 to 2500 MB across datasets.

4.2 Experimental Results

Non-Overlapping Scenario In Table 1, we present the node classification results for the non-overlapping scenario, characterized by a notably heterogeneous subgraph FL challenge. FedSheafHN stands out as it consistently outperforms other baseline approaches. FED-PUB, as our primary target baseline for subgraph PFL, achieves commendable results by identifying community structures via similarity estimation and selectively filtering irrelevant weights from diverse communities. However, in scenarios with many distinct clients and extreme heterogeneity, relying solely on similarity measures is insufficient for adequately inferring client relationships. Flow dynamically selects local and global model parameters based on the input instance. Although it performs well, it is not specifically designed for subgraph FL and does not fully exploit the underlying relationships

Table 2. Results on the overlapping node scenario. The reported results are mean and standard deviation over five different runs. The best and the second-best results are highlighted in bold and underlined, respectively. OOM refers to out-of-memory.

Methods	Cora		Citeseer		Pubmed	
	30 Clients	50 Clients	30 Clients	50 Clients	30 Clients	50 Clients
Local	71.65±0.12	75.45±0.51	64.54±0.42	66.68±0.44	80.72±0.16	80.54±0.11
FedAvg	63.84±2.57	57.98±0.06	66.11±1.50	58.00±0.29	83.11±0.03	82.24±0.73
FedProx	51.38±1.74	56.27±9.04	66.11±0.75	66.53±0.43	82.13±0.13	80.50±0.46
FedSage+	51.99±0.42	55.48±11.5	65.97±0.02	65.93±0.30	82.14±0.11	80.31±0.68
FGGP	62.59±0.49	53.50±0.48	57.50±0.39	52.90±0.53	71.70±0.82	70.49±0.43
FedPer	54.70±2.58	64.66±0.07	58.91±2.41	58.33±2.91	70.08±0.38	71.13±0.04
pFedHN	48.71±2.19	49.19±2.54	54.67±1.28	46.34±2.24	69.21±1.37	65.55±1.41
pFedGraph	<u>77.72±0.41</u>	<u>77.69±0.20</u>	69.60±0.11	<u>67.84±0.75</u>	83.12±0.37	82.60±0.27
FED-PUB	75.66±1.02	76.52±0.87	68.76±0.26	66.95±0.70	84.97±0.30	84.38±0.38
Flow	77.62±0.17	77.45±0.21	<u>70.86±0.10</u>	67.39±0.15	82.50±0.07	82.11±0.23
FedSheafHN (ours)	80.30±0.11	78.06±0.22	71.90±0.15	68.59±0.12	84.45±0.03	83.65±0.02

Methods	Amazon-Computer		Amazon-Photo		ogbn-arxiv	
	30 Clients	50 Clients	30 Clients	50 Clients	30 Clients	50 Clients
Local	64.65±1.09	68.28±1.02	72.60±0.78	80.68±1.48	61.32±0.04	60.04±0.04
FedAvg	68.99±3.97	67.69±0.12	83.74±0.72	75.59±0.06	49.91±2.84	52.26±1.02
FedProx	83.84±0.89	76.60±0.47	89.17±0.40	72.36±2.06	59.86±0.16	61.12±0.04
FedSage+	81.33±1.20	76.72±0.39	88.69±0.99	72.41±1.36	59.90±0.12	60.95±0.09
FGGP	70.44±1.65	64.04±1.25	75.01±0.51	62.40±1.50	OOM	OOM
FedPer	62.06±0.08	67.87±0.08	68.82±0.34	75.69±0.14	42.19±0.01	43.77±0.33
pFedHN	59.88±1.31	59.63±2.42	67.85±0.23	72.07±1.52	43.64±0.40	41.38±0.66
pFedGraph	76.77±1.53	74.46±0.42	77.07±0.69	87.81±1.96	59.29±0.39	58.96±0.56
FED-PUB	<u>88.40±0.80</u>	88.77±0.07	92.01±0.07	91.76±0.35	63.96±0.10	64.66±0.19
Flow	87.61±0.10	88.83±0.08	92.74±0.05	91.88±0.04	65.84±0.03	65.86±0.03
FedSheafHN (ours)	89.25±0.02	89.29±0.05	93.34±0.04	92.36±0.06	67.69±0.10	67.51±0.05

among clients. FedSheafHN enhances relationship inference and feature representation in highly heterogeneous scenarios, thus boosting the performance of HNs in creating personalized client models. Its adaptability to diverse and complex cases makes it a promising choice for addressing complexities in tough scenarios.

Overlapping Scenario The overlapping scenario, with lower heterogeneity as outlined in Table 2, still showcases FedSheafHN’s effectiveness across various datasets. Although its advantages are less pronounced compared to the non-overlapping scenario, the diverse feature representation of FedSheafHN is designed to address the intricacies of this setting. It consistently outperforms state-of-the-art baselines, highlighting its robustness and adaptability to varying degrees of heterogeneity, positioning it as a more reliable option.

Convergence Plots Fig. 4 illustrates the fast convergence of FedSheafHN, likely due to its ability to discern client cooperation and enable intelligent information sharing through data-driven client descriptions. Furthermore, the HNs, with learned attention and batch processing of all clients, efficiently generate model parameters and integrate global information.

Effectiveness of Personalization Our goal is to improve the accuracy of all clients by generating personalized models through sheaf collaboration. Effective collaboration should benefit all clients, regardless of heterogeneity in local subgraphs. To evaluate this, we measure the standard deviation of local accuracies across clients, where a lower value indicates more effective personalization. As shown in Table 3, FedSheafHN achieves the lowest standard deviation, demonstrating a more stable and balanced performance across all clients.

Generalization to New Clients We evaluate FedSheafHN on unseen clients without retraining or fine-tuning the shared model. Once $S(\cdot; \theta)$ and $H(\cdot; \varphi)$ are trained, we simply freeze θ and φ , initial-

Table 3. Mean and standard deviation of local accuracies across clients on the ogbn-arxiv dataset.

Methods	non-overlapping 20 clients	overlapping 30 clients
pFedGraph	56.01±16.10	59.13±12.60
FED-PUB	66.67±10.48	63.94±10.43
Flow	69.78±9.06	65.84±9.15
FedSheafHN (ours)	71.88±7.92	67.78±7.98

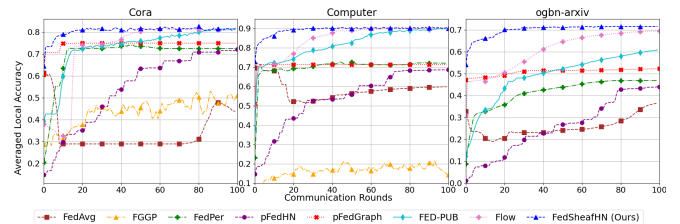


Figure 4. Convergence plots in the non-overlapping scenario (20 clients) across three datasets.

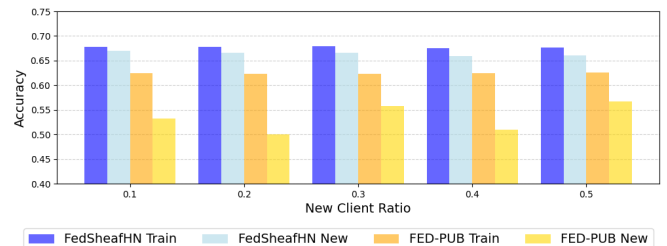


Figure 5. Generalization results on ogbn-arxiv dataset with 30 clients in overlapping scenario. "Train" indicates average test accuracy for trained clients, and "New" for newly joined clients with new client ratios from 0.1 to 0.5.

Table 4. Ablation studies of FedSheafHN on the ogbn-arxiv dataset.

Methods	non-overlapping 20 clients	overlapping 30 clients
Base model (FedAvg)	36.56	42.95
+ Hypernetwork	61.26	56.53
+ Collaboration graph	68.51	64.68
+ Sheaf diffusion	70.05	65.87
+ Attention	70.97	67.09
+ Dynamic embedding (ours)	71.87	67.89

Table 5. Different GNN models on collaboration graph.

Methods	non-overlapping 20 clients	overlapping 30 clients
w/o Sheaf diffusion ^a	69.75	65.66
w/ GCN ^b	69.86	65.96
w/ GAT	69.92	65.90
w/ Sheaf diffusion (ours)	71.87	67.89

^a Remove the “sheaf diffusion” part in FedSheafHN.^b Replace sheaf diffusion model with GCN.

ize the new client’s model, and train locally to derive graph-level embedding \mathbf{x}_{new} . As shown in Fig. 5, FedSheafHN achieves comparable accuracy for new clients with minimal performance reduction, requiring only one communication round for \mathbf{x}_{new} .

4.3 Ablation Studies

Effect of Each Module Table 4 shows our ablation study, adding components to the base model (FedAvg) to assess their impact. The results highlight the positive contributions of constructing collaboration graph (collaboration graph), dynamic embedding updates during training (dynamic embedding), sheaf diffusion for graph enhancement (sheaf diffusion), an improved batch-wise HNs (hypernetwork), and incorporating an attention layer in the HNs (attention). All components improve performance, with the collaboration graph and enhanced hypernetwork being most impactful. Notably, replacing the collaboration graph with one-hot client vectors in the “+ Hypernetwork” variant results in noticeably performance drop. The collaboration graph with client embeddings refines representations, enabling HNs to generate tailored model parameters.

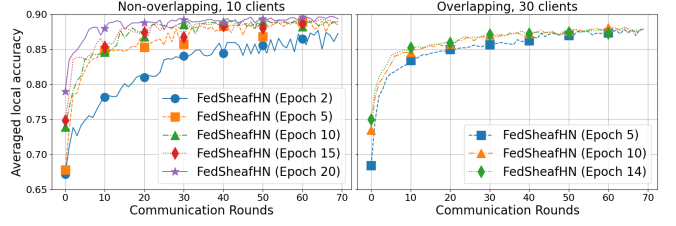
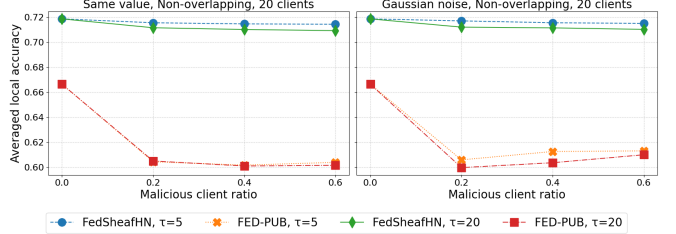
Effect of Alternative GNNs Table 5 shows that removing or replacing sheaf diffusion with other GNNs consistently results in lower performance. This highlights the effectiveness of sheaf diffusion in enhancing the collaboration graph by uncovering latent relationships.

Effect of Varying Local Epochs Fig. 6 shows that increasing local update steps T_c can cause local models diverging towards their subgraphs, highlighting the trade-off between local training and convergence. Thus, more local epochs do not always improve performance, and the optimal number varies by dataset.

4.4 Further Discussions

Computational Overhead Both sheaf collaboration and HNs run entirely on the server, so clients incur no extra computation compared to standard FL baselines. The only added communication is graph-level embedding, which introduces negligible overhead. As shown in Table 6, the server-side training time introduced by sheaf diffusion and HNs is modest and brings clear performance gains.

Moreover, increasing the number of clients does not add new trainable parameters on the server. The server training time increases by just 0.34% and 4.42% when scaling from 20 to 50 and 100 clients, respectively, indicating good scalability.

**Figure 6.** Performance on the Computer dataset with varying local epochs.**Figure 7.** Performance on the ogbn-arxiv dataset with malicious clients.**Table 6.** Server training time per communication round and total memory usage (ogbn-arxiv, 20 clients, non-overlapping scenario).

Method	Time (s)	Memory (MiB)
FedSheafHN	0.588	978
w/o Sheaf diffusion	0.559	974
w/ GCN	0.580	978
Base model (FedAvg)	0.130	970
+ Hypernetwork	0.407	974
50 clients	0.590	978
100 clients	0.614	980

Robustness to Malicious Clients Fig. 7 illustrates scenarios where malicious clients attempt to disrupt the training process by sending arbitrary graph-level or functional embeddings to the server, with malicious client ratios set at 0, 0.2, 0.4, and 0.6. Two types of embeddings are considered for the attack: (1) same-value parameters generated by $\mathbf{x}_i^{(ma)} = a\mathbf{I}_{d_{x_i}}$, where $\mathbf{I}_{d_{x_i}} \in \mathbb{R}^{d_{x_i}}$ is a vector of ones and $a \sim \mathcal{N}(0, \tau^2)$, and (2) Gaussian noise parameters generated by $\mathbf{x}_i^{(ma)} \sim \mathcal{N}(\mathbf{0}_{d_{x_i}}, \tau^2\mathbf{I}_{d_{x_i}})$ [23]. Compared to the subgraph FL baseline FED-PUB, which utilizes functional embeddings of the local GNNs using random graphs as inputs to compute similarities between clients and accordingly perform model aggregation, our method demonstrates greater resilience to malicious clients.

5 Conclusion

We have proposed FedSheafHN, a novel framework for personalized subgraph FL that centers on sheaf collaboration and HNs to address client heterogeneity. FedSheafHN proves highly effective in both non-overlapping and overlapping scenarios. Our theoretical analysis further ensures convergence and generalization guarantees, reinforcing the practical viability of the approach. Experimental results demonstrate its superior performance, fast convergence, effectiveness of personalization and ability to generalize to new clients. Our ablation studies emphasize the significant contributions of each component, especially the client graph-level embedding in constructing the collaboration graph. In general, FedSheafHN provides a promising strategy for effective collaborative learning while preserving the unique data characteristics of each client within a federated network.

References

- [1] N. Agarwal, P. Kairouz, and Z. Liu. The skellam mechanism for differentially private federated learning. *Advances in Neural Information Processing Systems*, 34:5052–5064, 2021.
- [2] M. G. Arivazhagan, V. Aggarwal, A. K. Singh, and S. Choudhary. Federated learning with personalization layers. *arXiv preprint arXiv:1912.00818*, 2019.
- [3] J. Baek, W. Jeong, J. Jin, J. Yoon, and S. J. Hwang. Personalized subgraph federated learning. In *International Conference on Machine Learning*, pages 1396–1415. PMLR, 2023.
- [4] J. Baxter. A model of inductive bias learning. *Journal of artificial intelligence research*, 12:149–198, 2000.
- [5] C. Bodnar, F. Di Giovanni, B. Chamberlain, P. Liò, and M. Bronstein. Neural sheaf diffusion: A topological perspective on heterophily and oversmoothing in gnns. *Advances in Neural Information Processing Systems*, 35:18527–18541, 2022.
- [6] A. Brock, T. Lim, J. M. Ritchie, and N. Weston. SMASH: one-shot model architecture search through hypernetworks. *arXiv preprint arXiv:1708.05344*, 2017.
- [7] J. M. Curry. *Sheaves, cosheaves and applications*. University of Pennsylvania, 2014.
- [8] M. Fey and J. E. Lenssen. Fast graph representation learning with pytorch geometric. *arXiv preprint arXiv:1903.02428*, 2019.
- [9] A. Ghosh, J. Chung, D. Yin, and K. Ramchandran. An efficient framework for clustered federated learning. *Advances in Neural Information Processing Systems*, 33:19586–19597, 2020.
- [10] J. Hansen and T. Gebhart. Sheaf neural networks. *arXiv preprint arXiv:2012.06333*, 2020.
- [11] F. Hanzely, S. Hanzely, S. Horváth, and P. Richtárik. Lower bounds and optimal algorithms for personalized federated learning. *Advances in Neural Information Processing Systems*, 33:2304–2315, 2020.
- [12] C. He, E. Ceyani, K. Balasubramanian, M. Annavaram, and S. Avestimehr. Spreadgnn: Serverless multi-task federated learning for graph neural networks. *arXiv preprint arXiv:2106.02743*, 2021.
- [13] W. Hu, M. Fey, M. Zitnik, Y. Dong, H. Ren, B. Liu, M. Catasta, and J. Leskovec. Open graph benchmark: Datasets for machine learning on graphs. *Advances in Neural Information Processing Systems*, 33:22118–22133, 2020.
- [14] Y. Huang, L. Chu, Z. Zhou, L. Wang, J. Liu, J. Pei, and Y. Zhang. Personalized cross-silo federated learning on non-iid data. In *Proceedings of the AAAI conference on Artificial Intelligence*, pages 7865–7873, 2021.
- [15] Y. Jiang, J. Konečný, K. Rush, and S. Kannan. Improving federated learning personalization via model agnostic meta learning. *arXiv preprint arXiv:1909.12488*, 2019.
- [16] G. Karypis. Metis: Unstructured graph partitioning and sparse matrix ordering system. *Technical report*, 1997.
- [17] D. Kinga, J. B. Adam, et al. A method for stochastic optimization. In *International Conference on Learning Representations*, 2015.
- [18] B. Klein, L. Wolf, and Y. Afek. A dynamic convolutional layer for short range weather prediction. In *Proceedings of the IEEE Conference on Computer Vision and Pattern Recognition*, pages 4840–4848, 2015.
- [19] S. Klocek, Ł. Maziarka, M. Wołczyk, J. Tabor, J. Nowak, and M. Śmieja. Hypernetwork functional image representation. In *International Conference on Artificial Neural Networks*, pages 496–510. Springer, 2019.
- [20] R. Lee, M. Kim, D. Li, X. Qiu, T. Hospedales, F. Huszár, and N. Lane. Fed12p: Federated learning to personalize. *Advances in Neural Information Processing Systems*, 36, 2024.
- [21] T. Li, A. K. Sahu, M. Zaheer, M. Sanjabi, A. Talwalkar, and V. Smith. Federated optimization in heterogeneous networks. *Proceedings of Machine learning and systems*, 2:429–450, 2020.
- [22] Y. Li, T. Wang, C. Chen, J. Lou, B. Chen, L. Yang, and Z. Zheng. Clients collaborate: Flexible differentially private federated learning with guaranteed improvement of utility-privacy trade-off. *arXiv preprint arXiv:2402.07002*, 2024.
- [23] S. Lin, Y. Han, X. Li, and Z. Zhang. Personalized federated learning towards communication efficiency, robustness and fairness. *Advances in Neural Information Processing Systems*, 35:30471–30485, 2022.
- [24] X. Ma, J. Zhang, S. Guo, and W. Xu. Layer-wised model aggregation for personalized federated learning. In *Proceedings of the IEEE/CVF conference on computer vision and pattern recognition*, pages 10092–10101, 2022.
- [25] J. McAuley, C. Targett, Q. Shi, and A. Van Den Hengel. Image-based recommendations on styles and substitutes. In *Proceedings of the 38th international ACM SIGIR conference on research and development in information retrieval*, pages 43–52, 2015.
- [26] B. McMahan, E. Moore, D. Ramage, S. Hampson, and B. A. y Arcas. Communication-efficient learning of deep networks from decentralized data. In *Artificial intelligence and statistics*, pages 1273–1282. PMLR, 2017.
- [27] A. Navon, A. Shamsian, G. Chechik, and E. Fetaya. Learning the pareto front with hypernetworks. *arXiv preprint arXiv:2010.04104*, 2020.
- [28] K. Panchal, S. Choudhary, N. Parikh, L. Zhang, and H. Guan. Flow: per-instance personalized federated learning. *Advances in Neural Information Processing Systems*, 36, 2024.
- [29] A. Paszke, S. Gross, F. Massa, A. Lerer, J. Bradbury, G. Chanan, T. Killeen, Z. Lin, N. Gimelshein, L. Antiga, et al. Pytorch: An imperative style, high-performance deep learning library. *Advances in Neural Information Processing Systems*, 32, 2019.
- [30] K. Pillutla, K. Malik, A.-R. Mohamed, M. Rabbat, M. Sanjabi, and L. Xiao. Federated learning with partial model personalization. In *International Conference on Machine Learning*, pages 17716–17758. PMLR, 2022.
- [31] J. Schneider and M. Vlachos. Personalization of deep learning. In *Proceedings of International Data Science Conference*, pages 89–96. Springer, 2021.
- [32] J. A. Scott, H. Zakerinia, and C. Lampert. Pefl: Personalized federated learning by learning to learn. In *12th International Conference on Learning Representations*, 2024.
- [33] P. Sen, G. Namata, M. Bilgic, L. Getoor, B. Galligher, and T. Eliassi-Rad. Collective classification in network data. *AI magazine*, 29(3):93–93, 2008.
- [34] A. Shamsian, A. Navon, E. Fetaya, and G. Chechik. Personalized federated learning using hypernetworks. In *International Conference on Machine Learning*, pages 9489–9502. PMLR, 2021.
- [35] O. Shchur, M. Mumme, A. Bojchevski, and S. Günnemann. Pitfalls of graph neural network evaluation. *arXiv preprint arXiv:1811.05868*, 2018.
- [36] R. She, Q. Kang, S. Wang, W. P. Tay, Y. L. Guan, D. N. Navarro, and A. Hartmannsgruber. Image patch-matching with graph-based learning in street scenes. *IEEE Transactions on Image Processing*, 32:3465–3480, 2023.
- [37] V. Smith, C.-K. Chiang, M. Sanjabi, and A. S. Talwalkar. Federated multi-task learning. *Advances in Neural Information Processing Systems*, 30, 2017.
- [38] Y. Tan, Y. Liu, G. Long, J. Jiang, Q. Lu, and C. Zhang. Federated learning on non-iid graphs via structural knowledge sharing. In *Proceedings of the AAAI conference on artificial intelligence*, pages 9953–9961, 2023.
- [39] G. Wan, W. Huang, and M. Ye. Federated graph learning under domain shift with generalizable prototypes. In *Proceedings of the AAAI Conference on Artificial Intelligence*, pages 15429–15437, 2024.
- [40] Z. Wang, X. Fan, J. Qi, H. Jin, P. Yang, S. Shen, and C. Wang. Fedgs: Federated graph-based sampling with arbitrary client availability. In *Proceedings of the AAAI Conference on Artificial Intelligence*, volume 37, pages 10271–10278, 2023.
- [41] D. J. Watts and S. H. Strogatz. Collective dynamics of ‘small-world’ networks. *nature*, 393(6684):440–442, 1998.
- [42] C. Wu, F. Wu, Y. Cao, Y. Huang, and X. Xie. FedGNN: Federated graph neural network for privacy-preserving recommendation. *arXiv preprint arXiv:2102.04925*, 2021.
- [43] H. Xie, J. Ma, L. Xiong, and C. Yang. Federated graph classification over non-iid graphs. *Advances in Neural Information Processing Systems*, 34:18839–18852, 2021.
- [44] Z. Xu, L. Yang, and S. Gu. Heterogeneous federated learning based on graph hypernetwork. In *International Conference on Artificial Neural Networks*, pages 464–476. Springer, 2023.
- [45] Y. Yan, S. Wang, F. Sun, and X. Tong. Personalized federated learning with multi-view geometry structure. *IEEE Internet of Things Journal*, 2024.
- [46] R. Ye, Z. Ni, F. Wu, S. Chen, and Y. Wang. Personalized federated learning with inferred collaboration graphs. In *International Conference on Machine Learning*, pages 39801–39817. PMLR, 2023.
- [47] C. Zhang, M. Ren, and R. Urtasun. Graph hypernetworks for neural architecture search. *arXiv preprint arXiv:1810.05749*, 2018.
- [48] J. Zhang, S. Guo, X. Ma, H. Wang, W. Xu, and F. Wu. Parameterized knowledge transfer for personalized federated learning. *Advances in Neural Information Processing Systems*, 34:10092–10104, 2021.
- [49] K. Zhang, C. Yang, X. Li, L. Sun, and S. M. Yiu. Subgraph federated learning with missing neighbor generation. *Advances in Neural Information Processing Systems*, 34:6671–6682, 2021.
- [50] K. Zhao, X. Li, Q. Kang, F. Ji, Q. Ding, Y. Zhao, W. Liang, and W. P. Tay. Distributed-order fractional graph operating network. *Advances in Neural Information Processing Systems*, 37:103442–103475, 2024.

A Appendix - Experimental Setups

A.1 Datasets

Table 7. Dataset statistics for the non-overlapping node scenario for both the original graph and its split subgraphs [3]. ‘‘Ori’’ denotes the original largest connected components in the graph. The clustering coefficient, reflecting node clustering within subgraphs, is calculated by averaging node coefficients [41]. Heterogeneity, indicating subgraph dissimilarity, is measured by the median Jensen-Shannon divergence of label distributions across subgraph pairs.

	Cora			Citeseer			Pubmed		
	Ori	10 Clients	20 Clients	Ori	10 Clients	20 Clients	Ori	10 Clients	20 Clients
# Classes		7			6			3	
# Nodes	2,485	249	124	2,120	212	106	19,717	1,972	986
# Edges	10,138	891	422	7,358	675	326	88,648	7,671	3,607
Clustering Coefficient	0.238	0.259	0.263	0.170	0.178	0.180	0.060	0.066	0.067
Heterogeneity	N/A	0.606	0.665	N/A	0.541	0.568	N/A	0.392	0.424

	Amazon-Computer			Amazon-Photo			ogbn-arxiv		
	Ori	10 Clients	20 Clients	Ori	10 Clients	20 Clients	Ori	10 Clients	20 Clients
# Classes		10			8			40	
# Nodes	13,381	1,338	669	7,487	749	374	169,343	16,934	8,467
# Edges	491,556	36,136	15,632	238,086	19,322	8,547	2,315,598	182,226	86,755
Clustering Coefficient	0.351	0.398	0.418	0.410	0.457	0.477	0.226	0.259	0.269
Heterogeneity	N/A	0.612	0.647	N/A	0.681	0.751	N/A	0.615	0.637

Table 8. Dataset statistics for the overlapping node scenario for both the original graph and its split subgraphs.

	Cora			Citeseer			Pubmed		
	Ori	30 Clients	50 Clients	Ori	30 Clients	50 Clients	Ori	30 Clients	50 Clients
# Classes		7			6			3	
# Nodes	2,485	207	124	2,120	177	106	19,717	1,643	986
# Edges	10,138	379	215	7,358	293	170	88,648	3,374	1,903
Clustering Coefficient	0.238	0.129	0.125	0.170	0.087	0.096	0.060	0.034	0.035
Heterogeneity	N/A	0.567	0.613	N/A	0.494	0.547	N/A	0.383	0.394

	Amazon-Computer			Amazon-Photo			ogbn-arxiv		
	Ori	30 Clients	50 Clients	Ori	30 Clients	50 Clients	Ori	30 Clients	50 Clients
# Classes		10			8			40	
# Nodes	13,381	1,115	669	7,487	624	374	169,343	14,112	8,467
# Edges	491,556	16,684	8,969	238,086	8,735	4,840	2,315,598	83,770	44,712
Clustering Coefficient	0.351	0.348	0.359	0.410	0.391	0.410	0.226	0.185	0.191
Heterogeneity	N/A	0.577	0.614	N/A	0.696	0.684	N/A	0.606	0.615

We present statistical analyses derived from six distinct benchmark datasets [33, 25, 35, 13]: Cora, CiteSeer, Pubmed, and ogbn-arxiv for citation graphs, as well as Computer and Photo for Amazon product graphs. These datasets serve as the foundation for our experimental investigations, covering both non-overlapping and overlapping and node scenarios, detailed in Tables 7 and 8. The table provides a comprehensive overview of key metrics for each subgraph, encompassing node and edge counts, class distribution, and clustering coefficients [3]. The clustering coefficient, indicating the extent of node clustering within individual subgraphs, is calculated by first determining the coefficient [41] for all nodes and subsequently computing the average. The heterogeneity, reflecting dissimilarity among disjoint subgraphs, is measured by calculating the median Jensen-Shannon divergence of label distributions across all subgraph pairs. These statistics offer a detailed understanding of the structural intricacies and relationships within the benchmark datasets utilized in the experiments. In partitioning datasets, we randomly allocate 40% of nodes for training, 30% for validation, and another 30% for testing across all datasets.

We delineate the procedure for partitioning the original graph into multiple subgraphs, tailored to the number of clients participating in FL. The METIS graph partitioning algorithm [16] is employed to effectively segment the original graph into distinct subgraphs, offering control over the number of disjoint subgraphs through adjustable parameters. In scenarios with non-overlapping nodes, each client is assigned a unique disjoint subgraph directly derived from the METIS algorithm output. For example, setting the METIS parameter to 10 results in 10 distinct disjoint subgraphs, each allocated to an individual client. Conversely, in scenarios involving overlapping nodes across subgraphs, the process begins by dividing the original graph into 6 and 10 disjoint subgraphs for configurations with 30 and 50 clients, respectively, utilizing the METIS algorithm. Subsequently, within each split subgraph, half of the nodes and their associated edges are randomly sampled, forming a subgraph assigned to a specific client. This iterative process is repeated 5 times, generating 5 distinct yet overlapped subgraphs for each split subgraph obtained from METIS. This meticulous approach ensures a varied yet controlled distribution of data across clients, accommodating both non-overlapping and overlapping node scenarios within the framework of FL.

A.2 Algorithm

Algorithm 1 FedSheafHN

Input: Communication rounds R , number of clients N , number of client local training rounds T_c , interval between client collaboration graph update r_{in} .

Initialization:

for client $i \in [N]$ **do**

 Initialize client model parameter $\omega_i = (\omega_{b,i}, \omega_{h,i})$.

 CLIENT-UPDATE(0, i , $\omega_{b,i}$)

end for

Server:

for communication round $r \in \{0, \dots, R\}$ **do**

if $(r \bmod r_{in}) == 0$ **then**

 Set $\mathbf{X}_0 = (\mathbf{x}_i^{(c)})_{i \in [N]}$ received from clients.

 Update G_s in (4) with received \mathbf{X}_0 .

else

 Set the current \mathbf{X}_0 to the value of \mathbf{X}_0 from the previous communication round.

end if

 Compute $\mathbf{X}_{T_s} = S(\mathbf{X}_0; \theta)$.

 Generate $\Omega_b^{(s)} = H(\mathbf{X}_{T_s}; \varphi)$ and transmit to clients.

for client i in $[N]$ **do**

 CLIENT-UPDATE(r , i , $\omega_{b,i}^{(s)}$)

end for

 Gradient descent update of θ via $\theta := \theta - \alpha \Delta \theta$.

 Gradient descent update of φ via $\varphi := \varphi - \beta \Delta \varphi$.

end for

Client:

procedure CLIENT-UPDATE(r , i , $\omega_{b,i}^{(s)}$)

 Set $\omega_{b,i} = \omega_{b,i}^{(s)}$.

for epoch $\in [T_c]$ **do**

 Gradient descent update of ω_i via $\omega_i := \omega_i - \gamma \nabla_{\omega_i} \mathcal{L}_i(\omega_i)$.

end for

if $(r \bmod r_{in}) == 0$ **then**

 Compute graph-level embedding $\mathbf{x}_i^{(c)}$ using (3) and transmit to the server.

end if

 Transmit $\Delta \omega_{b,i} := \omega_{b,i}^{(c)} - \omega_{b,i}^{(s)}$ to the server.

end procedure

A.3 Hyperparameters

The hyperparameter ranges used in our experiments are listed in Table 9.

Table 9. Hyperparameter ranges

Sheaf diffusion model	Learning rate	(0.02, 0.01, 0.001, 0.0001, 0.00001)
	Hidden channels	(5, 10, 20)
	Weight decay	0.0005
	Layer dropout	0-0.6
Hypernetworks	Learning rate	(0.02, 0.01, 0.001)
	Layer dropout	0.3
Client model	Learning rate	(0.02, 0.01, 0.001)
	Weight decay	0.0005
	Layer dropout	0-0.6

B Appendix - Convergence Proofs

Let $\omega_t = (\eta_t, \omega_{h,i,t}, i \in [N])$ denotes the parameters at communication round t . $g_{t,i,l}$ denotes stochastic gradient for client i at round t , local epoch l . Denote $\omega_{b,i} = M(\eta)$.

The overall objective is $\mathcal{L}(\omega) = \frac{1}{N} \sum_{i=1}^N \mathcal{L}_i(\omega_i)$, where

$$\begin{aligned} \mathcal{L}_i(G, \omega_i) &= \mathcal{L}_i(G, (\omega_{b,i}, \omega_{h,i})) \\ &= \mathcal{L}_i(G, (f_{i,1}(\omega_{b,i}), f_{i,2}(\omega_{h,i}))) \end{aligned}$$

B.1 Assumptions

Following the literature [32], we make the assumptions separately for each component.

- Bounded Gradients: there exist constants b_1, b_2, b_3 , such that

$$\begin{aligned} \|\nabla_{\omega_{b,i}} f_{i,1}(\omega_{b,i})\| &\leq b_1 \\ \|\nabla_{\omega_{h,i}} f_{i,1}(\omega_{h,i})\| &\leq b_2 \\ \|\nabla_y \omega_{b,i}\| &\leq b_3 \end{aligned}$$

- Smoothness: there exist constants L_1, L_4, L_5, L_7 , such that

$$\begin{aligned} \|\omega_{b,i} - \omega'_{b,i}\| &\leq L_1 \|y - y'\| \\ \|\nabla_{\omega_{h,i}} f_{i,2}(\omega_{h,i}) - \nabla_{\omega_{h,i}} f_{i,2}(\omega'_{h,i})\| &\leq L_4 \|\omega_{h,i} - \omega'_{h,i}\| \\ \|\nabla_{\omega_{b,i}} f_{i,1}(\omega_{b,i}) - \nabla_{\omega_{b,i}} f_{i,1}(\omega'_{b,i})\| &\leq L_7 \|\omega_{b,i} - \omega'_{b,i}\| \\ \|\nabla_y \omega_{b,i} - \nabla_y \omega'_{b,i}\| &\leq L_5 \|\eta - \eta'\| \end{aligned}$$

- Bounded Variance: there exists a constant σ_1 , such that

$$\mathbb{E} \|\nabla_{\omega_{b,i}} f_{i,1}(\omega_{b,i}) - \nabla_{\omega_{b,i}} \hat{f}_{i,1}(\omega_{b,i})\|^2 \leq \sigma_1^2$$

- Bounded Dissimilarity: there exists a constant L_G , such that with $\bar{\mathcal{L}}(\omega) = \frac{1}{N} \sum_{i=1}^N \mathcal{L}_i(\omega)$:

$$\frac{1}{N} \sum_{i=1}^N \mathbb{E} \|\nabla \mathcal{L}_i(\omega) - \nabla \bar{\mathcal{L}}(\omega)\|^2 \leq L_G^2$$

B.2 Convergence

Lemma 1. *There exists a constant L which $\nabla \mathcal{L}(\omega)$ is L -smooth.*

Proof. For each \mathcal{L}_i we have

$$\begin{aligned} \|\nabla_{\omega} \mathcal{L}_i(\omega_i) - \nabla_{\omega} \mathcal{L}_i(\omega'_i)\| &= \|\nabla_{\omega} \mathcal{L}_i(\omega_{b,i}, \omega_{h,i}) - \nabla_{\omega} \mathcal{L}_i(\omega'_{b,i}, \omega'_{h,i})\| \\ &= \|\nabla_{\omega_{b,i}} f_{i,1}(\omega_{b,i})^\top \nabla_{\eta} \omega_{b,i}^\top - \nabla_{\omega_{b,i}} f_{i,1}(\omega'_{b,i})^\top \nabla_{\eta} \omega'_{b,i}^\top\| \\ &\quad + \|\nabla_{\omega_{h,i}} f_{i,2}(\omega_{h,i})^\top \nabla_{\eta} \omega_{h,i}^\top - \nabla_{\omega_{h,i}} f_{i,2}(\omega'_{h,i})^\top \nabla_{\eta} \omega'_{h,i}^\top\| \\ &= \|\nabla_{\omega_{b,i}} f_{i,1}(\omega_{b,i})^\top \nabla_{\eta} \omega_{b,i}^\top - \nabla_{\omega_{b,i}} f_{i,1}(\omega_{b,i})^\top \nabla_{\eta} \omega'_{b,i}^\top\| \\ &\quad + \|\nabla_{\omega_{b,i}} f_{i,1}(\omega_{b,i})^\top \nabla_{\eta} \omega'_{b,i}^\top - \nabla_{\omega_{b,i}} \mathcal{L}_i(\omega'_i) \nabla_{\omega_{b,i}} f_{i,1}(\omega'_{b,i})^\top \nabla_{\eta} \omega'_{b,i}^\top\| \\ &\quad + \|\nabla_{\omega_{h,i}} f_{i,2}(\omega_{h,i})^\top \nabla_{\eta} \omega_{h,i}^\top - \nabla_{\omega_{h,i}} f_{i,2}(\omega'_{h,i})^\top \nabla_{\eta} \omega'_{h,i}^\top\| \\ &\leq b_2 L_5 \|\eta - \eta'\| + b_3 L_7 \|\omega_{b,i} - \omega'_{b,i}\| + L_4 \|\omega_{h,i} - \omega'_{h,i}\| \\ &= (b_2 L_5 + b_3 L_7) \|\eta - \eta'\| + L_4 \|\omega_{h,i} - \omega'_{h,i}\| \end{aligned}$$

Let $\omega_i = (\eta, \omega_{h,i})$, $L = \max\{b_2 L_5 + b_3 L_7, L_4\}$

$$\|\nabla_{\omega} \mathcal{L}_i(\omega_i) - \nabla_{\omega} \mathcal{L}_i(\omega'_i)\| \leq L \|\omega_i - \omega'_i\|$$

Therefore for \mathcal{L} we have

$$\begin{aligned}\|\nabla_{\omega}\mathcal{L}(\omega) - \nabla_{\omega}\mathcal{L}(\omega')\| &\leq \left\| \frac{1}{N} \sum_{i=1}^N \nabla_{\omega}\mathcal{L}_i(\omega) - \frac{1}{N} \sum_{i=1}^N \nabla_{\omega}\mathcal{L}_i(\omega') \right\| \\ &\leq L_2\|\eta - \eta'\| + \frac{1}{N} \sum_{i=1}^N L_2\|\omega_{h,i} - \omega'_{h,i}\| \\ &= L_2\|\omega - \omega'\|\end{aligned}$$

□

Lemma 2. For any step t and client i the following inequality holds:

$$\mathbb{E}_t\|\nabla\mathcal{L}_i(\omega_t) - \nabla_{\omega_{b,i}}f_{i,1}(\omega_{b,i}^t) - \beta \sum_{j=0}^{l-1} g_{t,i,j}(\omega_{b,i}^t) \nabla_{\eta_t}\omega_{b,i}^{t\top}\|^2 \leq 3L_7^2b_3^2\beta^2l^2(b_2^2 + \sigma_1^2).$$

Proof. Through the addition and subtraction of intermediate terms, followed by the application of the Cauchy–Schwarz inequality, we obtain

$$\begin{aligned}\mathbb{E}_t\|\nabla\mathcal{L}_i(\omega_t) - \nabla_{\omega_{b,i}}f_{i,1}(\omega_{b,i}^t) - \beta \sum_{j=0}^{l-1} g_{t,i,j}(\omega_{b,i}^t) \nabla_{\eta_t}\omega_{b,i}^{t\top}\|^2 \\ \leq 3\mathbb{E}\|\nabla_{\omega_{b,i}}f_{i,1}(\omega_{b,i}^t) - \nabla_{\omega_{b,i}}f_{i,1}(\omega_{b,i}^t) - \beta \sum_{j=0}^{l-1} g_{t,i,j}(\omega_{b,i}^t)\|^2 \|\nabla_{\eta_t}\omega_{b,i}^t\|^2 \\ \leq 3L_7^2b_3^2\beta^2\mathbb{E}\left\|\sum_{j=0}^{l-1} g_{t,i,j}(\omega_{b,i}^t)\right\|^2 \\ \leq 3L_7^2b_3^2\beta^2l^2(b_2^2 + \sigma_1^2)\end{aligned}$$

□

Lemma 3. For any step t the following inequality holds:

$$\mathbb{E}\langle\nabla\mathcal{L}(\omega_t), \omega_{t+1} - \omega_t\rangle \leq -\frac{3\beta T_c}{4}\mathbb{E}\|\nabla\mathcal{L}(\omega_t)\|^2 + L_7^2b_3^2\beta^3T_c^3(b_2^2 + \sigma_1^2) + \beta b_1^2$$

Proof.

$$\begin{aligned}\mathbb{E}\langle\nabla\mathcal{L}(\omega_t), \omega_{t+1} - \omega_t\rangle &\leq \langle\nabla_{\eta}\mathcal{L}(\omega_t), \eta_{t+1} - \eta_t\rangle + \frac{1}{N} \sum_{i=1}^N \langle\nabla_{\omega_{h,i}}\mathcal{L}(\omega_t), \omega_{h,i,t+1} - \omega_{h,i,t}\rangle \\ &= \mathbb{E}\left[\langle\nabla_{\eta}\mathcal{L}(\omega_t), -\frac{\beta}{N} \sum_{i=1}^N \sum_{l=1}^{T_c} g_{t,i,l}(\omega_{b,i,t}) \nabla_{\eta_t}\omega_{b,i,t}^{\top}\rangle\right] + \frac{1}{N} \sum_{i=1}^N \mathbb{E}\langle\nabla_{\omega_{h,i}}\mathcal{L}(\omega_t), \omega_{h,i,t+1} - \omega_{h,i,t}\rangle \\ &= \mathbb{E}_t\left[\langle\nabla_{\eta}\mathcal{L}(\omega_t), -\frac{\beta}{N} \sum_{i=1}^N \sum_{l=1}^{T_c} \nabla_{\omega_{b,i}}f_{i,1}\left(\omega_{b,i,t} - \beta \sum_{j=0}^{l-1} g_{t,i,j}(\omega_{b,i,t})\right) \nabla_{\eta_t}\omega_{b,i,t}^{\top}\rangle\right] \\ &\quad + \frac{1}{N} \sum_{i=1}^N \mathbb{E}\langle\nabla_{\omega_{h,i}}\mathcal{L}(\omega_t), \omega_{h,i,t+1} - \omega_{h,i,t}\rangle \\ &= \frac{\beta}{N} \sum_{i=1}^N \sum_{l=1}^{T_c} \mathbb{E}_t\left[\langle\nabla_{\eta}\mathcal{L}(\omega_t), \nabla_{\eta}\mathcal{L}_i(\omega_t) - \nabla_{\omega_{b,i}}f_{i,1}\left(\omega_{b,i,t} - \beta \sum_{j=0}^{l-1} g_{t,i,j}(\omega_{b,i,t})\right) \nabla_{\eta_t}\omega_{b,i,t}^{\top}\rangle\right] \\ &\quad + \frac{\beta}{N} \sum_{i=1}^N \sum_{l=1}^{T_c} \mathbb{E}_t\left[\langle\nabla\mathcal{L}(\omega_t), \nabla\mathcal{L}_i(\omega_t)\rangle\right] + \frac{1}{N} \sum_{i=1}^N \mathbb{E}\langle\nabla_{\omega_{h,i}}\mathcal{L}(\omega_t), \omega_{h,i,t+1} - \omega_{h,i,t}\rangle\end{aligned}$$

By definition $\mathcal{L}_{\omega} = \frac{1}{N} \sum_{i=1}^N \mathcal{L}_i(\omega_i)$, and by Young's inequality and Lemma 2 we have

$$\begin{aligned}
& \mathbb{E}\langle \nabla \mathcal{L}(\omega_t), \omega_{t+1} - \omega_t \rangle \\
& \leq \frac{\beta T_c}{4} \|\nabla_\eta \mathcal{L}(\omega_t)\|^2 + \frac{\beta}{N} \sum_{i=1}^N \sum_{l=1}^{T_c} \mathbb{E} \left\| \nabla_\eta \mathcal{L}_i(\omega_t) - \nabla_{\omega_{b,i}} f_{i,l}(\omega_{b,i,t}) - \beta \sum_{j=0}^{l-1} g_{t,i,j}(\omega_{b,i,t}) \nabla_{\eta_t} \omega_{b,i,t}^\top \right\|^2 \\
& \quad - \beta T_c \|\nabla_\eta \mathcal{L}(\omega_t)\|^2 + \frac{1}{N} \sum_{i=1}^N \mathbb{E} \langle \nabla_{\omega_{h,i}} \mathcal{L}(\omega_t), \omega_{h,i,t+1} - \omega_{h,i,t} \rangle \\
& \leq -\frac{3\beta T_c}{4} \mathbb{E} \|\nabla \mathcal{L}(\omega_t)\|^2 + \frac{\beta}{N} \sum_{i=1}^N \sum_{l=1}^{T_c} \left(3L_7^2 b_3^2 \beta^2 l^3 (b_2^2 + \sigma_1^2) \right) + \beta b_1^2 \\
& = -\frac{3\beta T_c}{4} \mathbb{E} \|\nabla \mathcal{L}(\omega_t)\|^2 + L_7^2 b_3^2 \beta^3 T_c^3 (b_2^2 + \sigma_1^2) + \beta b_1^2
\end{aligned}$$

□

Lemma 4. For any step t the following inequality holds:

$$\mathbb{E}[\|\eta_{t+1} - \eta_t\|^2] \leq \frac{4\beta^2 T_c}{N} \sigma_1^2 + 12\beta^4 L_7^2 b_3^2 T_c^4 (b_2^2 + \sigma_1^2) + \frac{4\beta^2 T_c^2}{N} L_G^2 + 4\beta^2 T_c^2 \mathbb{E} \left[\|\nabla \mathcal{L}(\omega_t)\|^2 \right].$$

Proof.

$$\begin{aligned}
\mathbb{E}[\|\eta_{t+1} - \eta_t\|^2] &= \mathbb{E} \left[\left\| -\frac{\beta}{N} \sum_{i=1}^N \sum_{l=1}^{T_c} g_{t,i,l}(\omega_{b,i}^t) \nabla_{\eta_t} \omega_{b,i}^t \right\|^2 \right] \\
&= \frac{\beta^2}{N^2} \mathbb{E} \left[\left\| \sum_{i=1}^N \sum_{l=1}^{T_c} g_{t,i,l}(\omega_{b,i}^t) \nabla_{\eta_t} \omega_{b,i}^t \right\|^2 \right] \\
&= \frac{\beta^2}{N^2} \mathbb{E} \left[\left\| \sum_{i=1}^N \sum_{l=1}^{T_c} \left(g_{t,i,l}(\omega_{b,i}^t) \nabla_{\eta_t} \omega_{b,i}^t - \nabla_{\omega_{b,i}} f_{i,l}(\omega_{b,i}^t) - \beta \sum_{j=0}^{l-1} g_{t,i,j}(\omega_{b,i}^t) \nabla_{\eta_t} \omega_{b,i}^t \right) \right. \right. \\
& \quad \left. \left. - \sum_{i=1}^N \sum_{l=1}^{T_c} \nabla_{\omega_{b,i}} f_{i,l}(\omega_{b,i}^t) - \beta \sum_{j=0}^{l-1} g_{t,i,j}(\omega_{b,i}^t) - \nabla \mathcal{L}_i(\omega_t) \right. \right. \\
& \quad \left. \left. + \sum_{i=1}^N \sum_{l=1}^{T_c} \left(\nabla \mathcal{L}_i(\omega_t) - \nabla \mathcal{L}(\omega_t) \right) + \sum_{i=1}^N \sum_{l=1}^{T_c} \nabla \mathcal{L}(\omega_t) \right\|^2 \right]
\end{aligned}$$

By Cauchy–Schwarz inequality we get

$$\begin{aligned}
\mathbb{E}[\|\eta_{t+1} - \eta_t\|^2] &\leq \frac{4\beta^2}{N^2} \mathbb{E} \left[\left\| \sum_{i=1}^N \sum_{l=1}^{T_c} g_{t,i,l}(\omega_{b,i}^t) \nabla_{\eta_t} \omega_{b,i}^t - \nabla_{\omega_{b,i}} f_{i,l}(\omega_{b,i}^t) - \beta \sum_{j=0}^{l-1} g_{t,i,j}(\omega_{b,i}^t) \nabla_{\eta_t} \omega_{b,i}^t \right\|^2 \right] \\
& \quad + \frac{4\beta^2}{N^2} \mathbb{E} \left[\left\| \sum_{i=1}^N \sum_{l=1}^{T_c} \left(\nabla_{\omega_{b,i}} f_{i,l}(\omega_{b,i}^t) - \beta \sum_{j=0}^{l-1} g_{t,i,j}(\omega_{b,i}^t) \nabla_{\eta_t} \omega_{b,i}^t - \nabla \mathcal{L}_i(\omega_t) \right) \right\|^2 \right] \\
& \quad + \frac{4\beta^2}{N^2} \mathbb{E} \left[\left\| \sum_{i=1}^N \sum_{l=1}^{T_c} \left(\nabla \mathcal{L}_i(\omega_t) - \nabla \mathcal{L}(\omega_t) \right) \right\|^2 \right] + \frac{4\beta^2}{N^2} \mathbb{E} \left[\left\| \sum_{i=1}^N \sum_{l=1}^{T_c} \nabla \mathcal{L}(\omega_t) \right\|^2 \right] \\
&\leq \frac{4\beta^2}{N^2} \sum_{i=1}^N \sum_{l=1}^{T_c} \mathbb{E} \left[\left\| g_{t,i,l}(\omega_{b,i}^t) \nabla_{\eta_t} \omega_{b,i}^t - \nabla_{\omega_{b,i}} f_{i,l}(\omega_{b,i}^t) - \beta \sum_{j=0}^{l-1} g_{t,i,j}(\omega_{b,i}^t) \nabla_{\eta_t} \omega_{b,i}^t \right\|^2 \right]
\end{aligned}$$

By Lemma 2, the bounded dissimilarity assumption and simplifying terms, we obtain

$$\begin{aligned}
\mathbb{E}[\|\eta_{t+1} - \eta_t\|^2] &\leq \frac{4\beta^2 T_c}{N} \sigma_1^2 + 4\beta^4 \cdot 3L_7^2 b_3^2 T_c^4 (b_2^2 + \sigma_1^2) \\
& \quad + \frac{4\beta^2 T_c^2}{N^2} \sum_{i=1}^N \mathbb{E} \left[\left\| \nabla \mathcal{L}_i(\omega_t) - \frac{1}{N} \sum_{i=1}^N \nabla \mathcal{L}_i(\omega_t) \right\|^2 \right] + 4\beta^2 T_c^2 \mathbb{E} \left[\|\nabla \mathcal{L}(\omega_t)\|^2 \right] \\
&\leq \frac{4\beta^2 T_c}{N} \sigma_1^2 + 12\beta^4 L_7^2 b_3^2 T_c^4 (b_2^2 + \sigma_1^2) + \frac{4\beta^2 T_c^2}{N} L_G^2 + 4\beta^2 T_c^2 \mathbb{E} \left[\|\nabla \mathcal{L}(\omega_t)\|^2 \right].
\end{aligned}$$

□

Theorem 1. Under standard assumptions of smoothness and boundedness, the optimization of FedSheafHN after T communication round satisfies

$$\frac{1}{T} \sum_{t=1}^T \mathbb{E} \|\nabla \mathcal{L}(\omega_t)\|^2 \leq \frac{(\mathcal{L}(\omega_0) - \mathcal{L}^*)}{\sqrt{NT}} + \frac{LL_1(16\sigma_1^2 + 8T_c L_G^2)}{T_c \sqrt{NT}} + \frac{16NL_7^2 b_3^2 b_2^2}{T} + \frac{(L+2)}{T_c} b_1^2$$

Proof. By smoothness of \mathcal{L} we have

$$\mathbb{E}[\mathcal{L}(\omega_{t+1}) - \mathcal{L}(\omega_t)] \leq \mathbb{E}[\langle \nabla \mathcal{L}(\omega_t), \omega_{t+1} - \omega_t \rangle] + \frac{L}{2} \mathbb{E} \left[\|\omega_{b,t+1} - \omega_{b,t}\|^2 + \frac{1}{N} \sum_{i=1}^N \|\omega_{h,i,t+1} - \omega_{h,i,t}\|^2 \right]$$

And by combining it with Lemma 3 and Lemma 4 and simplifying terms we get

$$\begin{aligned} \mathbb{E}[\mathcal{L}(\omega_{t+1}) - \mathcal{L}(\omega_t)] &\leq -\frac{3\beta T_c}{4} \mathbb{E} \|\nabla \mathcal{L}(\omega_t)\|^2 + L_7^2 b_3^2 \beta^3 T_c^3 (b_2^2 + \sigma_1^2) + \beta b_1^2 \\ &\quad + \frac{2\beta^2 T_c LL_1}{N} \sigma_1^2 + 6L\beta^4 L_7^2 b_3^2 T_c^4 L_1 (b_2^2 + \sigma_1^2) + \frac{2\beta^2 T_c^2 LL_1}{N} L_G^2 + 2\beta^2 T_c^2 LL_1 \mathbb{E}[\|\nabla \mathcal{L}(\omega_t)\|^2] + \frac{L}{2} \beta b_1^2 \\ &\leq \left(-\frac{3\beta T_c}{4} + 2L\beta^2 T_c^2 L_1 \right) \mathbb{E} \|\nabla \mathcal{L}(\omega_t)\|^2 + (\beta^3 T_c^3 + 6L\beta^4 T_c^4 L_1) L_7^2 b_3^2 b_2^2 \\ &\quad + \left(L_7 b_3^2 \beta^3 T_c^3 + 6L\beta^4 L_7^2 b_3^2 T_c^4 L_1 + \frac{2\beta^2 T_c LL_1}{N} \right) \sigma_1^2 + \left(\frac{L}{2} + 1 \right) \beta b_1^2 + \frac{2\beta^2 T_c^2 LL_1}{N} L_G^2 \end{aligned}$$

Therefore

$$\mathbb{E}[\mathcal{L}(\omega_{t+1}) - \mathcal{L}(\omega_t)] \leq -\frac{\beta T_c}{2} \mathbb{E} \|\nabla \mathcal{L}(\omega_t)\|^2 + 2\beta^3 T_c^3 L_7^2 b_3^2 b_2^2 + \frac{4\beta^2 T_c LL_1}{N} \sigma_1^2 + \left(\frac{L}{2} + 1 \right) \beta b_1^2 + \frac{2\beta^2 T_c^2 LL_1}{N} L_G^2$$

Hence

$$\mathbb{E} \|\nabla \mathcal{L}(\omega_t)\|^2 \leq \frac{2}{\beta T_c} \mathbb{E}[\mathcal{L}(\omega_t) - \mathcal{L}(\omega_{t+1})] + 4\beta^2 T_c^2 L_7^2 b_3^2 b_2^2 + \frac{8\beta LL_1}{N} \sigma_1^2 + \frac{L+2}{T_c} b_1^2 + \frac{4\beta T_c LL_1}{N} L_G^2$$

And

$$\frac{1}{T} \sum_{t=1}^T \mathbb{E} \|\nabla \mathcal{L}(\omega_t)\|^2 \leq \frac{2(\mathcal{L}(\omega_0) - \mathcal{L}^*)}{\beta T_c} + 4\beta^2 T_c^2 L_7^2 b_3^2 b_2^2 + \frac{8\beta LL_1}{N} \sigma_1^2 + \frac{L+2}{T_c} b_1^2 + \frac{4\beta T_c LL_1}{N} L_G^2$$

By setting $\beta = \frac{2\sqrt{N}}{T_c \sqrt{T}}$ we obtain

$$\frac{1}{T} \sum_{t=1}^T \mathbb{E} \|\nabla \mathcal{L}(\omega_t)\|^2 \leq \frac{(\mathcal{L}(\omega_0) - \mathcal{L}^*)}{\sqrt{NT}} + \frac{LL_1(16\sigma_1^2 + 8T_c L_G^2)}{T_c \sqrt{NT}} + \frac{16NL_7^2 b_3^2 b_2^2}{T} + \frac{(L+2)}{T_c} b_1^2$$

□

C Appendix - Generalization Proofs

Proof for Theorem 2.

Proof. Using Theorem 4 from [4] and the notation used in that paper, we obtain $M = \mathcal{O} \left(\frac{1}{N\epsilon^2} \log \left(\frac{C(\epsilon, H_c^N)}{\delta} \right) \right)$ where $C(\epsilon, H_c^N)$ is the covering number for H_c^N . In our case, expected loss is

$$\begin{aligned} \mathcal{L}(\omega_i, X_0) &= \frac{1}{N} \sum_{i=1}^N \mathbb{E}_{p_i} [\mathcal{L}_i(G_i; \omega_i)] \\ &= \frac{1}{N} \sum_{i=1}^N \mathbb{E}_{p_i} \left[\mathcal{L}_i \left(G_i; H(S(X_i^{(c)}), \theta), \varphi, \omega_{h,i} \right) \right]. \end{aligned}$$

We assume the following Lipschitz conditions hold:

$$\begin{aligned}
& |\mathcal{L}_i(G_i; \omega_i) - \mathcal{L}_i(G_i; \omega'_i)| \leq \mathcal{L} \|\omega_i - \omega'_i\| \\
& \|\omega_i - \omega'_i\| = \|(\omega_{b,i}, \omega_{h,i}) - (\omega'_{b,i}, \omega'_{h,i})\| \leq \|\omega_{b,i} - \omega'_{b,i}\| + \|\omega_{h,i} - \omega'_{h,i}\| \\
& \|H(x_i^{(T_s)}, \varphi) - H(x_i^{(T_s)}, \varphi')\| \leq L_H \|\varphi - \varphi'\| \\
& \|H(x_i^{(T_s)}, \varphi) - H(x_i^{(T_s)'}, \varphi)\| \leq L_{T_s} \|x_i^{(T_s)} - x_i^{(T_s)'}\| \\
& \|S(x_i^{(c)}, \theta) - S(x_i^{(c)}, \theta')\| \leq L_S \|\theta - \theta'\| \\
& \|S(x_i^{(c)}, \theta) - S(x_i^{(c)'}, \theta)\| \leq L_{T_o} \|x_i^{(c)} - x_i^{(c)'}\|
\end{aligned}$$

From the triangle inequality and the Lipschitz conditions, the distance is given by

$$\begin{aligned}
d &= \mathbb{E}_{P_i} \left[\frac{1}{N} \sum_{i=1}^N \mathcal{L}(\omega_i, X_0) - \frac{1}{N} \sum_{i=1}^N \mathcal{L}(\omega_i, X'_0) \right] \\
&\leq \frac{1}{N} \sum_{i=1}^N \mathbb{E}_{P_i} \left[\left| \mathcal{L}(h(\varphi, x_i^{(T_s)}), \omega_{h,i}; G_i) - \mathcal{L}(h(\varphi', x_i^{(T_s)}), \omega_{h,i}; G_i) \right| \right] \\
&\leq L \cdot \left\| h(\varphi, x_i^{(T_s)}) - h(\varphi', x_i^{(T_s)'}) \right\| + L \cdot \|\omega_{h,i} - \omega'_{h,i}\| \\
&\leq L \cdot \left(\|h(\varphi, x_i^{(T_s)}) - h(\varphi, x_i^{(T_s)'})\| + \|h(\varphi, x_i^{(T_s)'}) - h(\varphi', x_i^{(T_s)'})\| \right) + L \cdot \|\omega_{h,i} - \omega'_{h,i}\| \\
&\leq L \cdot L_{T_s} \cdot \|x_i^{(T_s)} - x_i^{(T_s)'}\| + L \cdot L_H \cdot \|\varphi - \varphi'\| + L \cdot \|\omega_{h,i} - \omega'_{h,i}\| \\
&\leq L \cdot L_{T_s} \cdot \|S(X_0; \theta) - S(X'_0; \theta')\| + L \cdot L_H \cdot \|\varphi - \varphi'\| + L \cdot \|\omega_{h,i} - \omega'_{h,i}\| \\
&\leq L \cdot L_{T_s} \cdot L_{T_o} \cdot \|X_0 - X'_0\| + L \cdot L_{T_s} \cdot L_S \cdot \|\theta - \theta'\| + L \cdot L_H \cdot \|\varphi - \varphi'\| + L \cdot \|\omega_{h,i} - \omega'_{h,i}\|.
\end{aligned}$$

If each of the parameters $\theta, \varphi, \omega_{h,i}$ and each embedding X_0 can be approximated within $\frac{\varepsilon}{4L(L_{T_s}(L_S + L_{T_o}) + L_H + 1)}$ by a corresponding point, then the resulting set forms an ε -covering under the metric d . From here we get

$$\log(C(\varepsilon, H^2)) = \mathcal{O} \left((Nd_i + d_\theta + d_\varphi + d_{\omega_{h,i}}) \log \left(\frac{RL(L_{T_s}(L_S + L_{T_o}) + L_H + 1)}{\varepsilon} \right) \right).$$

Let $L_s = L_{T_s} \cdot (L_S + L_{T_o})$. The bound expand to

$$\begin{aligned}
& \mathcal{O} \left(\frac{Nd_i + d_\theta + d_\varphi + d_{\omega_{h,i}}}{N\varepsilon^2} \log \left(\frac{RL(L_{T_s}(L_S + L_{T_o}) + L_H + 1)}{\varepsilon} \right) + \frac{1}{N\varepsilon^2} \log \frac{1}{\delta} \right) \\
&= \mathcal{O} \left(\left(d_i + \frac{d_\theta + d_\varphi + d_{\omega_{h,i}}}{N} \right) \frac{1}{\varepsilon^2} \log \left(\frac{RL(L_s + L_H + 1)}{\varepsilon} \right) + \frac{1}{N\varepsilon^2} \log \frac{1}{\delta} \right).
\end{aligned}$$

□